ChemPhysChem

Research Article
doi.org/10.1002/cphc.202400086

Chemistry Europe
European Chemical Societies Publishing

www.chemphyschem.org

Wetting Effect Induced Depletion and Adsorption Layers: Diffuse Interface Perspective

Haodong Zhang[+],[a, b] Hongmin Zhang[+],[a, b] Fei Wang,*[a, b] and Britta Nestler[a, b, c]

When a multi-component fluid contacts arigid solid substrate, the van der Waals interaction between fluids and substrate induces a depletion/adsorption layer depending on the intrinsic wettability of the system. In this study, we investigate the depletion/adsorption behaviors of A–B fluid system. We derive analytical expressions for the equilibrium layer thickness and the equilibrium composition distribution near the solid wall, based on the theories of de Gennes and Cahn. Our derivation is verified through phase-field simulations, wherein the substrate wettability, A–B interfacial tension, and temperature are systematically varied. Our findings underscore two pivotal mechanisms governing the equilibrium layer thickness. With an increase in the wall free energy, the substrate wettability dominates the layer formation, aligning with de Gennes' theory. When the interfacial tension increases, or temperature rises, the layer formation is determined by the A–B interactions, obeying Cahn's theory. Additionally, we extend our study to non-equilibrium systems where the initial composition deviates from the binodal line. Notably, macroscopic depletion/adsorption layers form on the substrate, which are significantly thicker than the equilibrium microscopic layers. This macroscopic layer formation is attributed to the interplay of phase separation and Ostwald ripening. We anticipate that the present finding could deepen our knowledge on the depletion/adsorption behaviors of immiscible fluids.

1. Introduction

When a droplet possessing an equilibrium composition is deposited onto a solid substrate in the proximity of another immiscible fluid, an apparent contact angle, denoted as θ, forms at the triple junction of fluid-fluid-solid[1–4] (see Figure 1). Conversely, an initial composition deviating from the equilibrium value in the fluids often results in a layered structure near the solid surface.[5–9] Simultaneously, the off-equilibrium liquid solution tends to decompose into two immiscible phases. Such layered structures proximal to the solid substrate are discernible in both metal and polymer solutions. In polymer solutions, this layered structure is referred to as the depletion/adsorption layer,[10–13] as extensively investigated by de Gennes[14] and many other researchers.[15–18] The present study aims to illuminate the depletion/adsorption layer from the perspective of wetting effects through the diffuse interface concept.

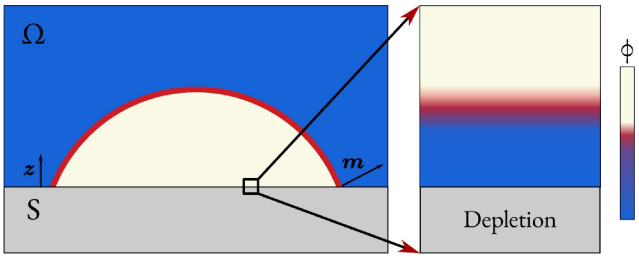

Figure 1. Schematic of an A–B binary fluid system amid the domain Ω contacting the substrate surface *S* colored in grey. The normal directions of the substrate and A–B interface are denoted by ***z*** and ***m***, respectively. The zoom-in sketches the depletion of component A by the substrate. The color bar depicts the composition of A represented by ϕ.

The physical origin of the depletion/adsorption layer is as follows. The thermodynamic equilibrium of the two immiscible bulk phases delineates the corresponding equilibrium bulk compositions within the respective fluid phases. Considering the thermodynamic equilibrium between the fluid phases and the solid substrate, the equilibrium composition in the fluid phase can differ from that results from liquid-liquid equilibrium.[1,19–21] In essence, treating the solid substrate as an inert object, as in Young's law, disrupts the symmetry at the solid-fluid interface, resulting in the accumulation or dispersion of species on the solid substrate. This asymmetry can be comprehended as a distinction in the formulation of the bulk free energy from the wall free energy. Specifically, the intermolecular force with attractive and repulsive interactions on the solid-fluid interface deviates from that inside the fluid bulk and at the fluid-fluid interface, leading to a surface composition macroscopically differing from the bulk value in the fluid phase.

[a] *H. Zhang,[+] H. Zhang,[+] F. Wang, B. Nestler*
Institute of Applied Materials-Microstructure Modelling and Simulation, Karlsruhe Institute of Technology, Straße am Forum 7, 76131 Karlsruhe, Germany
E-mail: fei.wang@kit.edu

[b] *H. Zhang,[+] H. Zhang,[+] F. Wang, B. Nestler*
Institute of Nanotechnology, Karlsruhe Institute of Technology, Hermann-von-Helmholtz-Platz 1, 76344 Eggenstein-Leopoldshafen, Germany

[c] *B. Nestler*
Institute of Digital Materials Science, Karlsruhe University of Applied Sciences, Moltkestraße 30, 76133 Karlsruhe, Germany

[+] *These authors contributed equally.*

Theoretical studies and analyses of experimental results predominantly rely on Cahn's critical point wetting theory,[19] with additional studies encompassing.[17] Cahn's theory is advantageous in explaining the discontinuity in the thickness of the depletion layer with temperature, known as the wetting transition temperature. However, a lingering question remains: whether this discontinuity in thickness arises from the discontinuity in surface composition or from the discontinuity in the apparent contact angle.[22] The pivotal factor for the formation of the depletion/adsorption layer lies in the difference between surface composition and bulk composition, which leads to a continuous and distorted composition profile from the surface to the bulk of the fluids. The distorted composition profile culminates in a surface excess at the solid-fluid interface.

While various models have already explored the depletion/adsorption layer,[17] a diffuse interface model has not yet been employed to scrutinize its formation mechanism and thickness. Within the diffuse interface theory for wetting phenomena, prevalent models[23–28] assume identical composition on the surface and in the bulk of the fluids. The identical bulk and surface composition is achieved by utilizing the associated wall free energy and the bulk free energy with minima at the same composition. While these models efficiently capture Young's contact angle for droplets with equilibrium composition, they fall short in investigating the depletion/adsorption layer. In the present work, we aim to derive closed forms for the thickness of the depletion/adsorption layer in terms of the wall free energy parameters.

Another aspect yet to be clarified is the wettability of the system associated with the depletion/adsorption mechanism. Previous studies have primarily focused on the scenarios where the solute molecules, either depleted or adsorbed, are fully miscible with the solvent matrix. These studies typically emphasize the impact of the solute-substrate interactions on the depletion mechanism, while treating the solvent matrix merely as a container for the solute molecules. In other words, the Young's contact angle associated with the depletion mechanism has not been clarified in previous works. A layered structure near the solid surface does not necessarily imply only two possible θ values, 0° for depletion or 180° for adsorption. In this study, we highlight the influence of wettability on the depletion/adsorption effect by taking the solvent-substrate interactions into consideration. Particularly, we heed the depletion/adsorption behaviors of the solute which is not fully miscible with the solvent, but gets separated from the solvent matrix via spinodal decomposition. This non-equilibrium initial state is beyond the scope of the equilibrium theory by de Gennes and Cahn, and results in a macroscopic depletion/adsorption layer magnitudes thicker than the microscopic equilibrium layer discussed in previous researches. Because of $0^\circ < \theta < 180^\circ$, the macroscopic depletion/adsorption layer may undergo fluid dynamics instability, forming a droplet structure via Rayleigh-Plateau instability[29,30] and subsequently establishing the Young's contact angle. The breakup of layered liquid structures has been comprehensively studied in Ref. [31] and is out of the scope of the current work. We anticipate our elucidation on the macroscopic and microscopic depletion/adsorption layers can deepen previous understanding on the depletion/adsorption mechanism.

The rest of the manuscript is structured as follows. Section 2 presents the diffuse interface model and introduces two approaches to calculate the depletion/adsorption layer thickness. In Section 3, we derive calculations for the wettability of the system associated with the depletion/adsorption layer. Section 4 compares numerical simulation results with the theory presented in Section 2. Section 5 sheds light on the formation of the depletion/adsorption layer when phase separation occurs inside the bulk fluid. The manuscript is concluded in Section 6.

2. Depletion/Adsorption Layer

2.1. Model Description

We consider a binary liquid solution consisting of components A and B; the solution contacts a solid wall in the domain Ω (see Figure 1). Upon demixing, the liquid solution results in two immiscible phases, say, a component A-rich phase and a component B-rich phase. To describe the thermodynamic equilibrium, we formulate the free energy functional of the system $\mathcal{F}$ as

$$\mathcal{F} = \int_\Omega [f_b + \kappa(\nabla\phi)^2] \mathrm{d}\Omega + \int_S f_w \,\mathrm{d}S. \tag{1}$$

The parameter ϕ depicts the local volume fraction of component A. The bulk free energy f_b takes the regular solution formulation as

$$f_b/f^* = \tfrac{T}{T_r}[\phi \ln\phi + (1-\phi)\ln(1-\phi)] + \chi\phi(1-\phi). \tag{2}$$

The bulk free energy density is scaled by the reference free energy density $f^* = R_g T_r / v_m$, with R_g, T_r, and v_m denoting universal gas constant, reference temperature, and molar volume, respectively. For brevity, we choose units such that $f^* = 1\mathrm{e}6\,\mathrm{N/m^2}$. The parameter T stands for absolute temperature and χ depicts the intermolecular potential accounting for the short-range van der Waals force of species A and B. The gradient energy coefficient κ is determined by the A–B interfacial tension as

$$\sigma = \int_{-\infty}^{\infty} 2\kappa \left(\frac{\mathrm{d}\phi}{\mathrm{d}\boldsymbol{m}}\right)^2 \mathrm{d}m = \int_{-\infty}^{\infty} 2\,\Delta f \,\mathrm{d}m = \int_{\phi_1}^{\phi_2} 2\sqrt{\kappa \Delta f}\,\mathrm{d}\phi, \tag{3}$$

where the vector $\boldsymbol{m}$ stands for the normal direction of the interface of the A-rich and B-rich phase; see Figure 1. The Landau potential reads $\Delta f = f_b(\phi) - \mu\phi$ in which the chemical potential is defined as $\mu = \delta F/\delta\phi = \partial f_b/\partial\phi - 2\kappa\nabla^2\phi$. The equilibrium compositions in the B-rich and A-rich phases are denoted by ϕ_1 and ϕ_2, respectively; see Figure 2(I), which are solved by the common tangent construction based on the following two criteria.

(I) Identical chemical potentials μ in the A-rich phase and the B-rich phase:

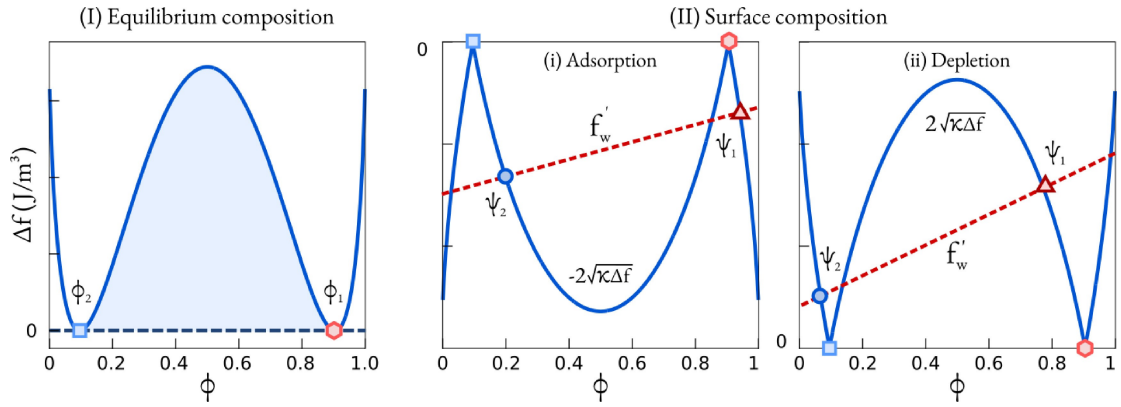

Figure 2. (I) Equilibrium compositions of A–B binary system at Landau potential $\triangle f = 0$. Blue square: ϕ_2 with B-rich; red hexagon: ϕ_1 with A-rich. (II) Surface composition ψ_s follows Eq. (7). (i) Adsorption case: ψ_1 (triangle) for A-rich phase and ψ_2 (circle) for B-rich phase. (ii) Depletion case.

$$\mu_1 = f_b^{'}(\phi_1) = \mu_2 = f_b^{'}(\phi_2).$$

(II) Identical Landau potential $\Delta f = f_b - \mu\phi$ in both phases:

$$f_b(\phi_1) - \mu_1\phi_1 = f_b(\phi_2) - \mu_2\phi_2.$$

Note that the condition (I) of equal chemical potential is not sufficient for the thermodynamic equilibrium. The basic reason is that the extensive property of the internal energy has not been taken into account in (I). The solution of the equations system (I) and (II) does not have a closed form. We solve this equation system numerically via the Newtonian iteration.

The last surface integral in Eq. (1) depicts the wall free energy resulting from the interaction between the liquid solution and the solid substrate *S*. To account for the repulsive and attractive interaction between the liquid and the solid wall, we adopt the following expression for the wall free energy density[1,20,32]

$$f_w/f_w^* = \frac{1}{2}\gamma_2\,\psi^2 + \gamma_1\psi + \gamma_0, \tag{4}$$

where the reference wall free energy $f_w^* = f^* v_m^{1/3}$. ψ denotes the local volume fraction of A species on the substrate. The physical meaning of the coefficients γ_2 and γ_1 is provided in Ref..[32] The constant γ_0 is an arbitrary reference value which does not affect the following discussion.

The substrate can either adsorb or repel the A/B molecules, forming the depletion/adsorption layers which depend on the sign of $f_w^{'}(\psi)$, as demonstrated in the following.

2.2. Surface Composition

In this Section, we focus on the depletion/adsorption phenomena at the thermodynamic equilibrium state, which is derived via the variational approach[4,23] on the solid wall $(\delta\mathcal{F}/\delta\psi)_S = 0$, leading to the boundary condition on *S*[21,28]

$$2\kappa\,\frac{d\psi}{dz} = f_w^{'} = \gamma_2\,\psi + \gamma_1, \tag{5}$$

where **z** denotes the substrate normal direction; see Figure 1. To establish a stable A–B interface, the gradient energy coefficient κ must be positive, so that Eq. 3 has . The gradient energy coefficient κ may depend on the composition and is assumed to be a constant for simplicity in the current work. Notably, the adsorption and depletion of A species by the substrate correspond to $(d\Psi/dz)|_{z=0} < 0$ and $(d\Psi/dz)|_{z=0} > 0$, respectively. Thus, according to Eq. 5, the depletion/adsorption is determined by the sign of $f_w^{'}(\Psi)$. For the adsorption layer of the component A on the substrate, we have $f_w^{'}(\Psi) < 0$; and for the depletion layer with $f_w^{'}(\psi) > 0$.

In addition, we derive the equilibrium surface composition ψ to compute $f_w^{'}(\psi)$. This can be calculated by the coupling of boundary condition with the bulk region Ω in which the thermodynamic equilibrium states follow

$$\frac{\partial f_b}{\partial\phi} = 2\,\kappa\,\frac{d^2\phi}{dz^2}.$$

Multiplying both sides by $\partial\phi/\partial z$ and integrating from the substrate layer $z = 0$ to $z = h$, we obtain

$$f_b(\phi(h)) - f_b(\psi_s) = \kappa(\frac{d\phi}{dz})^2|_{z=0}^{z=h}. \tag{6}$$

Here, we have assumed that the concentration in the layer on top of the surface layer is identical to the surface composition. Also, it is noteworthy that at the position infinitely far away from the substrate $z = h \to +\infty$, the composition gradient approaches 0 inside the fluid bulk region, yielding

$$f_b(\phi_1) = f_b(\psi_s) - \kappa(\frac{d\phi}{dz})^2|_0.$$

Then we arrive at

$$\frac{d\phi}{dz}|_{z=h} = \pm\sqrt{\frac{f_b(\phi) - f_b(\phi_1)}{\kappa}}. \tag{7}$$

Combining with Eq. (5), we have

$$\pm 2\sqrt{\kappa \Delta f(\psi)} = f_w'(\psi), . \tag{8}$$

where $\Delta f(\psi) = f_b(\psi) - f_b(\phi_1)$ is shown in Figure 2(I). The "+" and "−" signs represent the depletion and adsorption cases, respectively. In this way, the surface compositions are obtained as the intersections marked by the blue circles and red triangles in Figure 2(II).

2.3. Layer Thickness

Next, we propose two approaches to calculate the depletion/adsorption layer thickness d as

$$d = \int_{\psi_s}^{\phi_b} 1/(\mathrm{d}\psi/\mathrm{d}z)\mathrm{d}\psi. \tag{9}$$

Apparently, the solution of Eq. (9) is a logarithm type of function with infinite width of its rise/decay to the equilibrium bulk composition φ_b. Therefore, due to the resolution of the simulation mesh, instead of Eq. (9), we express the half-value width starting from substrate $z = 0$ to the position with $\phi_{1/2} = (\psi_s + \psi_b)/2$ as

$$d_{1/2} = \int_{\psi_s}^{\phi_{1/2}} 1/(\mathrm{d}\psi/\mathrm{d}z)\mathrm{d}\psi. \tag{10}$$

2.3.1. De Gennes' Approach

Substituting the boundary condition Eq. (5) into Eq. (10), the layer thickness reads

$$d_{1/2} = \frac{2\kappa}{|\gamma_2|} \ln \frac{\gamma_2 \phi_{1/2} + \gamma_1}{\gamma_2 \psi_s + \gamma_1}, \tag{11}$$

The composition ψ_s denotes the equilibrium value on the substrate by Eq. (8) with Cahn's theory.[19] When $\phi_b < \phi_{1/2} < \psi_s$, we have the adsorption case, while $\phi_b > \phi_{1/2} > \psi_s$ denotes the depletion scenario. Moreover, if the bulk composition φ_b equates the surface composition ψ_s, the depletion/adsorption layer vanishes. It is probably the reason why most previous phase-field models fail to capture the depletion/adsorption layer; in these models, the bulk composition is always identical to the surface composition. By integrating the wetting boundary condition, Eq. (5) in the normal direction **z**, we obtain the exponential profile of ψ as

$$\psi(z) = (\psi_s - \psi_b) \exp\left(\frac{z}{\alpha}\right) + \psi_b, \tag{12}$$

in which the factor $\alpha = 2\kappa(\psi_s - \psi_b)/(\gamma_2 \psi_s + \gamma_1)$ has a unit of length and scales the thickness of the depletion/adsorption layer.

2.3.2. Cahn's Approach

Substituting Eq. (7) into Eq. (9), we obtain the depletion/adsorption layer thickness d as

$$d_{1/2} = \pm \int_{\psi_s}^{\phi_{1/2}} \sqrt{\frac{\kappa}{\Delta f(\phi)}}\mathrm{d}\phi + C, \tag{13}$$

where the "+" and "−" signs correspond to the depletion and adsorption cases, respectively. Note that, an integral constant C appears because of the approximation adopted to derive Eq. (6) in which the free energy density term $f_b(\psi_s)$ is not correct. The constant C fixes the derivations of the simulated layer thickness with the theoretical value by Eq. (10) and is obtainable from the simulation. Moreover, Eq. (13) is only valid with the existence of depletion/adsorption layers. If $\psi_s = \phi_{1/2} = \phi_b$, the gradient term $\mathrm{d}\phi/\mathrm{d}z = 0$, and we can immediately conclude zero depletion/adsorption layer thickness without performing the integration. Distinct from de Gennes' approach, the ϕ profile can only be solved numerically. Since Eqs. (7) and (13) are derived based on the Cahn-Hilliard model, the composition distribution follows the solution of the Cahn-Hilliard equation, which can be represented by the hyperbolic tangent function as

$$\phi(z) = k_1 \tanh(k_2 z + k_3) + k_0, \tag{14}$$

in which the parameters k_0, k_1, k_2, and k_3 need to be numerically calculated with the following boundary conditions

$$\phi(0) = \psi_s, \quad \phi(\infty) = \phi_b,$$
$$\frac{\mathrm{d}\phi}{\mathrm{d}z}|_{z=0} = f_w' = \sqrt{\frac{f_b(\psi_s) - f_b(\phi_b)}{\kappa}}.$$

3. Intrinsic Wettability

Most often in experiments, a layered structure is observed near the solid substrate, especially for polymer solutions. This is because the initial composition in the liquid deviates from the equilibrium value. Because of the surface-directed spinodal decomposition, we arrive in a metastable state, forming an depletion/adsorption layer. Noteworthily, the layered structure does not indicate an intrinsic Young's contact angle of 0° or 180°. When an A-rich droplet with an equilibrium composition is initially placed on top of the substrate in the surrounding of the B-rich phase, we obtain the apparent contact angle, which is characterized by Young's contact angle. More suffice to say, the depletion/adsorption layer must be described within the framework of knowing intrinsic wettability. In this Section, we derive the calculation of the intrinsic wettability in terms of the parameters γ_1 and γ_2.

We integrate the wetting boundary condition from ψ_1 to ψ_2 as

$$\int_{\psi_1}^{\psi_2} 2\kappa \frac{\mathrm{d}\psi}{\mathrm{d}z}\mathrm{d}\psi = f_w(\psi_2) - f_w(\psi_1) \tag{15}$$

where ψ_1 and ψ_2 indicate the surface composition in the A-rich phase and the B-rich phase, respectively. We divide the integral $[\psi_1, \psi_2]$ into three sub-regions $[\psi_1, \phi_1]$, $[\phi_1, \phi_2]$, and $[\phi_2, \psi_2]$. The middle integral $[\phi_1, \phi_2]$ can be reduced to

$$\int_{\phi_1}^{\phi_2} 2\kappa \frac{\mathrm{d}\psi}{\mathrm{d}z}\mathrm{d}\psi = \int_{\phi_1}^{\phi_2} 2\kappa \frac{\mathrm{d}\phi}{\mathrm{d}m}\cos\theta\,\mathrm{d}\phi = \sigma\cos\theta. \tag{16}$$

Here, we have applied the geometrical relation $(\mathrm{d}\phi/\mathrm{d}m)\cos\theta = \mathrm{d}\psi/\mathrm{d}z$ and the definition of the A–B interfacial tension σ according to Eq. (3). The integrals in the other two sub-regions can be combined with the wall free energy. When defining the A-solid interfacial energy γ_A and the B-solid interfacial energy γ_B as

$$\gamma_{\mathrm{A/B}} \quad = f_w(\psi_{1/2}) + \int_{\psi_s}^{\phi_{1/2}} 2\kappa \frac{\mathrm{d}\psi}{\mathrm{d}z}\mathrm{d}\psi \tag{17}$$

we obtain the wettability of the system as

$$\sigma\cos\theta = \gamma_B - \gamma_A. \tag{18}$$

The result is consistent with Young's law.

4. Numerical Model

To simulate the depletion/adsorption of the A–B binary system in this work, we use the composition of component A, namely ϕ to distinguish A from B inside the bulk region Ω, so that the composition of component B is $1-\phi$, while applying ψ to represent the composition of component A on the substrate *S*. To establish the equilibrium depletion/adsorption layer, the spatiotemporal evolution of ϕ and ψ follows the Cahn-Hilliard equation with the natural wetting boundary condition as[20,33]

$$\frac{\partial\phi}{\partial t} = \nabla\cdot(\mathcal{M}\nabla\mu + \boldsymbol{\xi}),\ \text{in}\ \Omega, \tag{19}$$

$$\frac{\partial\psi}{\partial t} = \tau\left(2\kappa\nabla\psi\cdot\mathbf{n} + f_w^{'}\right),\ \text{on}\ S. \tag{20}$$

In Eq. (19), the kinetic parameter inside the bulk, namely the mobility, $\mathcal{M} = (D_0/f^*)\,\phi(1-\phi)$ takes the Onsager's relation[34] with the interdiffusivity D_0. The noise amplitude $\boldsymbol{\xi}$ follows the fluctuation-dissipation theorem[35] with

$$\langle\boldsymbol{\xi}(\mathbf{x},t),\boldsymbol{\xi}(\mathbf{x}',t')\rangle = \frac{2\mathcal{M}f^*}{\Delta t}\,\delta(\mathbf{x}-\mathbf{x}')\delta(t-t'),$$

in which $\Delta t = 0.001$ is the time step of the simulation and δ denotes the Dirac's delta. While in Eq. (20), the kinetic parameter on the substrate τ is fixed as 0.01 which scales the evolution speed of the surface composition towards the equilibrium.[21,23]

The kinetic equations Eqs. (19) and (20) are discretized by the finite difference method (see Ref. [22, 36]) with Message Passing Interface (MPI) techniques. By selecting the characteristic length $x^* = 1\mathrm{e}-8m$, reference diffusivity $D^* = 1\mathrm{e}-9\mathrm{m}^2/s$, as well as $f^* = 1\mathrm{e}6\mathrm{N/m}^2$, the equations are non-dimensionalized in the same way as Ref. [34]. The numerical convergence of the model has been comprehensively discussed in our previous study.[20,22,28] The simulations are performed on the parallel computer bwUniCluster of Baden-Wuerttemberg equipped with Intel Xeon Gold CPUs in the environment of Red Hat Enterprise.

5. Results and Discussion

In this Section, we discuss three pivotal factors that exert significant influence on the adsorption and depletion behaviors in the binary A–B system. These factors encompass (I) the wall free energy f_w, (II) the interfacial tension between components A and B, σ, and (III) the prevailing temperature *T*. In the following discussion, we will concentrate initially on the depletion of component A; the adsorption scenario will be addressed at the end of this Section.

5.1. Wall Free Energy

In the initial part of our analysis, we direct our attention to the impact of wall free energy on the depletion behavior. According to Eq. (11) and Eq. (13), the depletion layer thickness $d_{1/2}$ is intricately linked to the surface composition ψ_s. The graphical representation in Figure 3(I) elucidates that as the wall free energy f_w increases with a concurrent rise in γ_2, the derivative of wall free energy f_w to the composition ϕ (colored lines) undergoes augmentation. Consequently, this elevation leads to a reduction in the surface composition ψ_s, denoted by the colored dots. Thus, we suggest that the depletion behavior is modified by the alterations in the substrate wettability.

To validate this suggestion, a homogeneous A–B solution with the equilibrium composition $\phi = 0.9727$ at the temperature of $T = 1$ is brought into direct contact with the substrate. Initially setting the constant parameter $\gamma_1 = 0.5$, Figure 4(I) portrays that the blue-colored depletion layer thickens as γ_2 rises. A scrutiny of the composition profile along the *z* direction reveals that the variation in surface composition at $z = 0$ primarily accounts for the expansion of the depletion layer. With γ_2 increasing from 0.1 to 1.0, the surface composition ψ_s decreases from 0.956 to 0.914, while the equilibrium composition ϕ_b within the bulk region ($z > 10$) remains unaltered. This observation aligns seamlessly with the schematic illustration in Figure 3(I). The compositional disparity between ψ_s and φ_b establishes a diffuse interface in the *z* direction where the composition gradually changes from ψ_s to ϕ_b. Notably, a larger composition difference results in a broader interface, yielding a thicker depletion layer.

A series of simulations for various values of γ_1 and γ_2 is conducted; the simulation results are shown in Figure 4(I), where the depletion layer thickness is juxtaposed with both de Gennes and Cahn's theories. For configurations characterized by low wall free energy (small γ_2 and γ_1 values), the thickness $d_{1/2}$ from simulations exhibits commendable agreement with

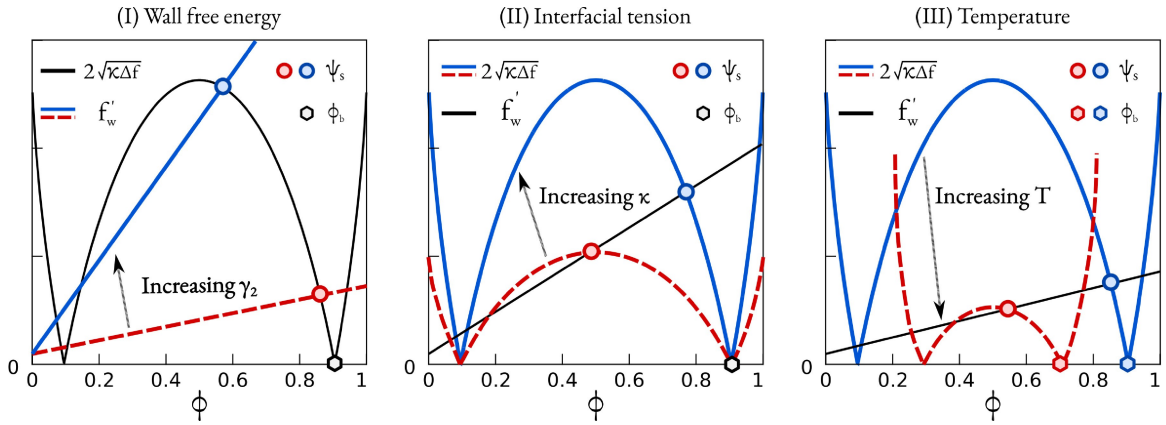

Figure 3. Schematic equilibrium conditions of A–B binary system. (I) The surface composition ψs (colored dots) decreases with increasing wall free energy f_w by enlarging γ_2. (II) The surface composition ψ_s (colored dots) decreases with increasing A–B interfacial tension by enlarging κ. In (I) and (II), the equilibrium composition ϕ_b (black hexagon) is unchanged. (III) Both the surface composition ψ_s (colored dots) and the equilibrium compositions ϕ_b (colored hexagons) decrease with increasing temperature T.

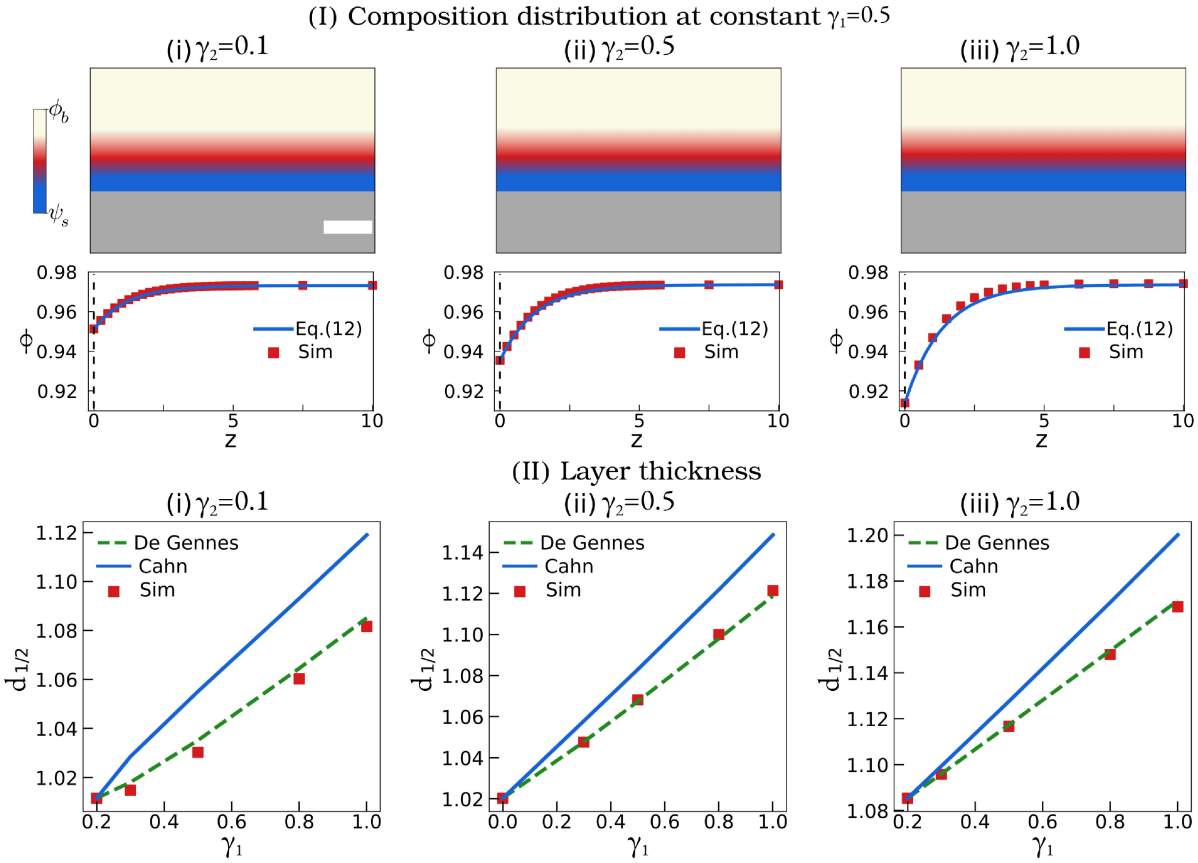

Figure 4. The depletion behavior of the A–B binary system influenced by the wall free energy by changing the parameters γ_1 and γ_2 in Eq. (4). (I) The component A composition distributions at constant $\gamma_1 = 0.5$ for various γ_2: (i) 0.1; (ii) 0.5; (iii) 1.0. Upper row: ϕ distributions; lower row: ϕ profile along the z direction. The color bar measures the ϕ value and the white scale bar denotes 5. (II) The depletion layer thickness $d_{1/2}$ with varying wetting ability parameter γ_1 at fixed γ_2 in Eq. (4), (i) $\gamma_2 = 0.1$; (ii) $\gamma_2 = 0.5$; (iii) $\gamma_2 = 1.0$.

both approaches. As the wall free energy intensifies, $d_{1/2}$ manifests a closer conformity to de Gennes' theory. This observation is in line with the composition profile in Figure 4(I) where ϕ follows the exponential relation with z, as postulated by de Gennes in Ref. [14]. This underscores that the depletion behavior becomes increasingly contingent on substrate properties, assuming a more pivotal role than the interactions between A–B species.

In addition, examining the equilibrium condition at the substrate (Eq. (5)) and our simulation, it becomes apparent that the composition gradient $d\phi/dz$ amplifies in the proximity of the substrate with an escalating γ_2. Significantly, in accordance

with Eq. (6), the augmentation in $d\phi/dz$ precipitates an antecedent increase in the A–B free energy f_b, which is proportionally scaled by the interfacial tension parameter κ. Consequently, the ensuing part will scrutinize the influence of interfacial tension on the depletion behavior.

5.2. Interfacial Tension

Based on the phase-field model employed in this study, the interfacial tension σ between components A and B is proportionally scaled by the parameter κ, as specified in Eq. (3). To investigate the impact of σ on the depletion layer, the following simulation parameters are adopted. The simulation commences with a homogeneous A–B solution owning an initial composition $\phi = 0.9727$ that is placed in contact with the substrate. The wall free energy f_w is fixed with $\gamma_1 = 0.3$ and $\gamma_2 = 0.5$, ensuring the formation of the depletion layer of component A on the substrate.

As illustrated in the schematic equilibrium condition in Figure 3(I), an increase in κ prompts the elevation of the w-shaped curve $2\sqrt{\kappa\Delta f}$. This results in a rightward shift of the colored intersection dots. Consequently, the surface composition ψ_s increases, while the equilibrium bulk composition ϕ_b remains unchanged (denoted by the black hexagon). Although the surface composition experiences an augmentation with κ, the compositional disparity between ψ_s and ϕ_b decreases, leading to an expansion of the transition region and the formation of a thicker depletion layer.

As depicted in the upper row of Figure 5(I), with an increase in κ from 3.2 to 40, the thickness of the depletion layer doubles. Conversely, in the lower row, the composition difference between ψ_s and ϕ_b decreases with κ. The composition profile (ϕ, marked by red squares) exhibits a broader transition region (depletion layer) with increasing κ. The ϕ profile shows a hyperbolic tangent function, as fitted by the blue solid line, which is consistent with de Gennes' results.[14] This stands in contrast to the wall free energy-dominated depletion behavior discussed in Sec. 5.1, where the thickness of the depletion layer shows a positive correlation with $\phi_b - \psi_s$. This result suggests an alternative mechanism governing the depletion behavior. The thickness of the depletion layer is not solely influenced by the A-substrate interaction but also hinges on the A–B interactions within the fluid system. With the increase in κ, the free energy of the mixture f_b follows a parabolic increase with $d\phi/dz$, as stated in Eq. (6). Therefore, even a small variation in composition near the substrate leads to a substantial increase in f_b. To minimize the total energy of the system, the composition profile along the z direction tends to flatten itself, thereby reducing the term $\kappa(d\phi/dz)^2$. Consequently, the transition region from ψ_s to ϕ_b thickens, and the dominance of interfacial tension becomes pronounced in the determination of the depletion layer thickness.

Furthermore, in Figure 5 (II), we compare the depletion layer thickness $d_{1/2}$ from simulations (red squares) with Cahn's theory (blue solid line) and de Gennes' theory (green dashed line). A closer adherence to Cahn's theory indicates an interfacial tension-dominated depletion behavior, which sharply contrasts the observations in the wall free energy-dominated scenario discussed in Sec. 5.1 referring to Figure 4(I).

5.3. Temperature

In addition to the wall free energy and interfacial tension, temperature T emerges as another pivotal factor exerting a substantial impact on depletion behaviors. As elucidated by the schematic equilibrium condition in Figure 3(II), an increase in T induces a decrement in the w-shaped curve $2\sqrt{\kappa\Delta f}$, resulting in a leftward shift of the colored intersection dots. By these means, the surface composition ψ_s decreases, accompanied by a simultaneous reduction in the equilibrium bulk composition ϕ_b, as denoted by the black hexagons. The dependence of the depletion layer thickness on temperature introduces a level of complexity beyond that observed in previous scenarios. To explore the temperature effect, we make the assumption that the wall free energy f_w is temperature-independent, thereby maintaining $\gamma_1 = 0.3$ and $\gamma_2 = 0.5$ to streamline the discussion.

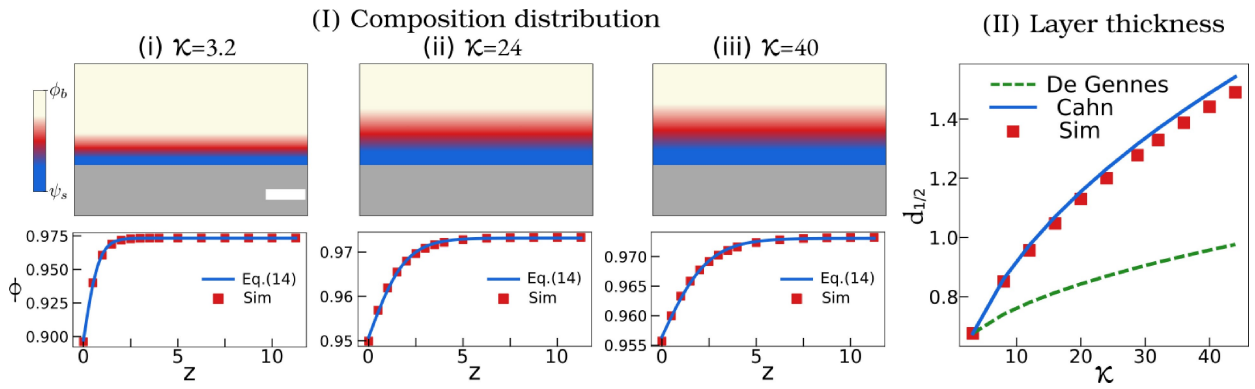

Figure 5. The depletion behavior of the A–B binary system influenced by the A–B interfacial tension. The wall free energy is fixed with $\gamma_1 = 0.3$, $\gamma_2 = 0.5$. (I) The component A composition distributions for various interfacial tension parameters κ: (i) 3.2; (ii) 24; (iii) 40. Upper row: ϕ distributions; lower row: ϕ profile along the z direction. The color bar measures the ϕ value and the white scale bar denotes 5. (II) The depletion layer thickness $d_{1/2}$ with increasing interfacial tension parameter κ. The simulated thickness is compared with theoretical values. Blue solid line: Cahn's approach according to Eq. (11); green dashed line: de Gennes' approach according to Eq. (13).

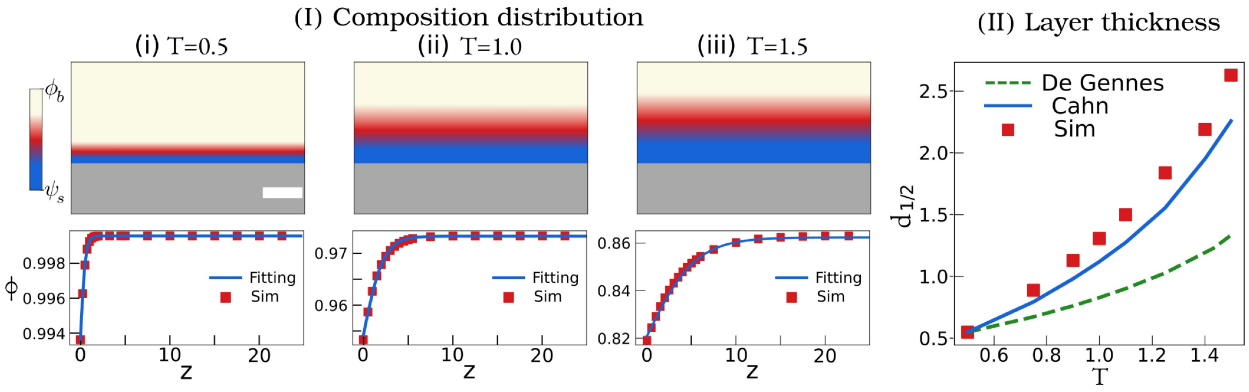

Figure 6. Simulation results for the thickness of depletion layer with different temperatures, specifically $T = 0.5$, 1, and 1.5. The depletion layer thickness positively correlates with temperature, indicating an increase in the depletion layer as the temperature rises. The white scale bar denotes 5.

The physical reason for this assumption is that the short-range van der Waals interaction of fluid-solid has a weak dependence on the temperature. The interfacial tension parameter κ is held constant at 3.2. Despite the constant values for both f_w and κ, the temperature still has a significant impact on the depletion behaviors. This mechanism unfolds through three interconnected aspects. As the temperature T increases, (i) the equilibrium composition ϕ_b within the bulk region declines, dropping from 0.9998 at $T = 0.5$ to 0.8623 at $T = 1.5$, as depicted in Figure 6(I). (ii) The surface composition ψ_s diminishes in a more obvious manner than ϕ_b, decreasing from 0.9931 at $T = 0.5$ to 0.8153 at $T = 1.5$. This leads to an augmentation in the composition difference $\phi_b - \psi_s$ with T. (iii) Simultaneously, the derivative of the free energy $\mathrm{d}f_w/\mathrm{d}\psi$ exhibits a monotonic decline with T. This implies that the composition gradient in the depletion layer $\mathrm{d}\phi/\mathrm{d}z$ also experiences a drastic reduction with rising T. Consequently, the free energy of the mixture f_b, proportional to $\kappa(\mathrm{d}\phi/\mathrm{d}z)^2$ diminishes.

Through the combination of these three facets, the depletion layer thickness $d_{1/2}$ increases with T, a mechanism akin to the collaborative influence of both the wall free energy-dominated and interfacial tension-controlled depletion behaviors. Consequently, the simulated $d_{1/2}$ surpasses the theoretical calculation derived from both Cahn and de Gennes' theory, as illustrated in Figure 6(II).

The preceding discussions and conclusions primarily address the specifics of the depletion layer, with a distinct focus on elucidating the underlying mechanisms. The adsorption behavior, although crucial, has not been explicitly demonstrated in this context. To facilitate the adsorption of component A, a straightforward adjustment involves setting $\gamma_1 = -0.3$ and $\gamma_2 = -0.5$ in the simulations. The symmetric nature of the free energy of the A–B system f_b about $\phi = 0.5$, as depicted in Figure 2(I), ensures that the interchange of A and B molecules can neither alter the interactions nor change surface tension. Consequently, the adsorption of A is effectively equivalent to the depletion of B. It is worth noting that for certain polymer systems characterized by asymmetric free energy,[20,37,38] the adsorption of A may not be synonymous with the depletion of B. However, the methodology employed for investigating adsorption remains consistent. For the sake of conciseness and to avoid redundancy, the specific adsorption case involving the adoption of $\gamma_1 = -0.3$ and $\gamma_2 = -0.5$ is not expounded upon in this work.

6. Perspective for Phase Separation and Macroscopic Layered Structure

In the previous Section, we discuss the depletion effect of the equilibrium cases, where the initial composition in the liquid is on the binodal line. In the following, we will investigate the depletion/adsorption of the A–B binary fluids system for the initial state far away from equilibrium. We consider the A–B system as before and compute the phase diagram as shown in Figure 7. The blue solid binodal line denotes the equilibrium composition inside the fluid bulk without substrate and curvature effect. The red dashed line encloses the spinodal region inside which the phase separation can be triggered by

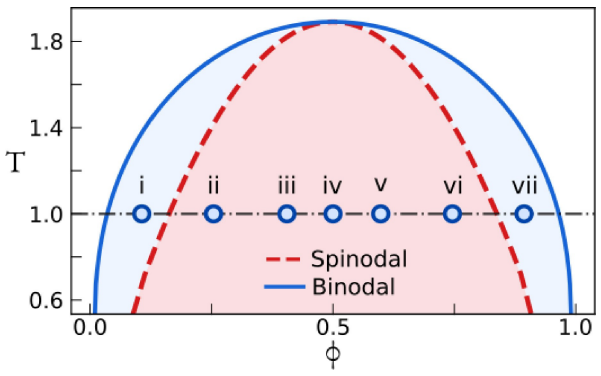

Figure 7. Phase diagram of A–B system illustrating binodal and spinodal compositions, represented by solid blue and dashed red lines, respectively. Phase separation within the pink spinodal region can be induced by thermal noise. The subsequent phase separation simulations are conducted at $T = 1.0$, with initial compositions as $\phi = 0.10$, 0.25, 0.40, 0.50, 0.60, 0.75, and 0.90, represented by blue circle points (i)–(vii), respectively.

the thermal noise with $\xi = (0.001, 0.001)$ in 2-dimensional simulations. Without the thermal noise, phase separation can not be observed. Here, we fix the temperature at $T = 1.0$ and simulate the initial compositions ranging from $\phi = 0.1$ to 0.9 which are marked by the sequence green dots in Figure 7. The simulations are performed both on the hydrophobic and hydrophilic substrates. The wettability is controlled by setting the wall free energy with $\gamma_1 = 0.3$ and $\gamma_2 = 0.5$ for hydrophobic and $\gamma_1 = -0.3$ and $\gamma_2 = -0.5$ for hydrophilic cases, resulting in a contact angle of 120.9° and 59.1°, respectively.

As shown in Figure 8, for both hydrophilic and hydrophobic cases, if the initial composition is out of the pink-colored spinodal region in Figure 7; see case (i) and (vii), phase separation will not take place and no macroscopic liquid layer is formed. It is worth emphasising that the surface composition effect manifests in all cases from (i) to (vii). Specifically, examining the region in direct contact with the substrate enclosed by the white dashed line in Figure 8, the microscopic depletion/adsorption layer still exists, as indicated by the simulation results corresponding to the equilibrium scenario depicted Figures 4–6.

Once entering the spinodal region, the white A-rich layer is formed on the hydrophilic substrate, and blue B-rich is formed on the hydrophobic. For the hydrophilic case, the predominant factor for the adsorption on the substrate is the surface composition effect, leading to the fusion of the adsorption layer and the A-rich phase layer. Consequently, the thickness of the adsorption layer on the substrate in the off-equilibrium

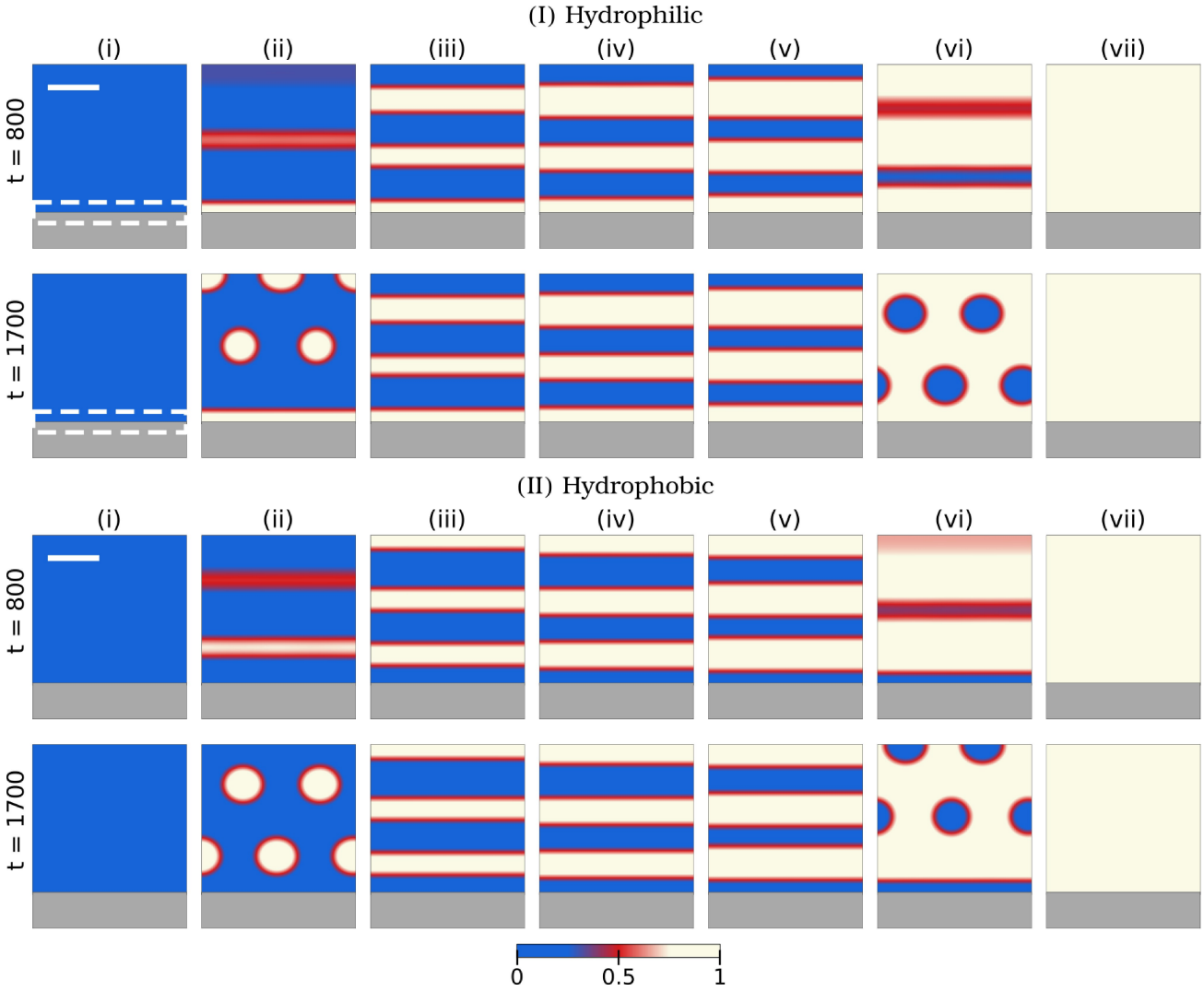

Figure 8. Simulation results of phase separation are presented in panels (i) to (vii), where the initial composition of the A component is set as $\phi = 0.10$, 0.25, 0.40, 0.50, 0.60, 0.75, and 0.90. The upper panel (I) and lower panel (II) correspond to the hydrophilic and hydrophobic substrate, respectively. Wettability is controlled by setting the wall free energy, with values of ($\gamma_1 = 0.3$, $\gamma_2 = 0.5$) for hydrophobic and ($\gamma_1 = -0.3$, $\gamma_2 = -0.5$) for hydrophilic cases, resulting in a contact angle of 120.9° and 59.1°, respectively. The white scale bar represents 100, and the colorbar indicates the composition of component A. In panels (ii)–(vi), the initial composition within the spinodal region leads to phase separation. For (I) and (II), the hydrophilic/hydrophobic wetting substrate induces the formation of an A-rich adsorption layer and a B-rich depletion layer, respectively. The establishment of A-rich/B-rich circles in (ii) and (vi) is attributed to thermal noise. The adsorption layer thickness in (I)(ii) for the hydrophilic case at time 1700 is greater than that at $t = 800$. The difference is due to the significantly large curvature of the circles compared to the adsorption plane layer, leading to the adsorption of A into the adsorption layer. The result for the hydrophobic case in (II)(vi) aligns with the conclusions.

simulation exceeds that discussed above in the equilibrium simulation. It is important to emphasize that in this context, the establishment of the macroscopic adsorption layer (i.e., the complete wetting state) is ascribed to another local energy minimum of the system. As elucidated by Whyman et al.,[39] considering a droplet with a constant volume, the total interfacial energy E of the system is a function of the contact angle θ, and its derivative is expressed as:

$$\frac{dE}{d\theta} = K[(\gamma_B - \gamma_A) - \sigma \cos\theta] \sin\theta, \quad (21)$$

where K is a material parameter with $K \neq 0$. γ_A, γ_B, and σ are interface tensions between A phase and solid, B phase and solid, and A–B phases, respectively. Attaining the local minimum of the system, $dE/d\theta = 0$ is required and fulfilled when $(\gamma_B - \gamma_A) - \sigma \cos\theta = 0$ or $\sin\theta = 0$. The former one corresponds to the local minimum of partial wetting (i.e., a droplet with a contact angle 59.1°), and Young's law is rigorously derived. The latter case is analogous to the local minimum of a complete wetting with $\theta = 0^\circ$ in this adsorption scenario. In Figure 8(I), from (ii) to (vi), the composition of A increases in the initial state and the thickness of the A-rich layer also increases. In this manner, this A-rich layer is also the adsorption layer of A. Compared with the simulation in Figures 4–6, this adsorption layer is magnitude thicker than the layer formed in the equilibrium composition.

The breakup of the A-rich phase layer and the subsequent formulation of the droplet shape are illustrated in Figure 8(I)(ii) at $t = 1700$. It is noteworthy to emphasize that the surface composition effect enhances the adsorption effect and the breakup is not observed on the substrate. The curvature of the A-rich droplet is much greater than that of the A-rich adsorption plane layer. Over time, the A composition is absorbed into the A-rich adsorption layer, namely the Ostwald ripening effect. Consequently, the thickness of the adsorption layer in Figure 8(I)(ii) at $t = 1700$ is thicker than that in Figure 8(I)(ii) at $t = 800$. Additionally, as the composition of A increases, Figure 8(I)(vi) at $t = 1700$ is not distinguished compared to $t = 800$, when the A-rich phase layer breaks up into spherical droplet shape.

Moreover, in the context of the hydrophobic scenario, the phase separation exhibits substantial concordance with those mentioned in the hydrophilic conditions. As illustrated in Figure 8(II), the B-rich depletion layer decreases from (ii) to (vi), as the composition of A rises. In Figure 8(II)(vi), the thickness of the depletion layer with a B-rich circle at t = 1700 is thicker than that at t = 800.

7. Conclusions

In conclusion, we have extensively examined the formation of the depletion/adsorption layer in a binary fluid system directly interfacing with a substrate. Leveraging the theoretical frameworks proposed by de Gennes and Cahn, we have derived expressions for the depletion/adsorption layer thickness as a function of the composition, interfacial tension, temperature, and wall free energy parameters. Additionally, we obtain theoretical equilibrium composition profiles parallel to the substrate's normal direction for both de Gennes and Cahn's approaches.

Employing the phase-field method, we have conducted simulations to scrutinize the depletion behavior of equilibrium A–B binary fluids under varying wall free energy parameters, interfacial tension, and temperature. Our findings reveal two distinct mechanisms influencing the depletion/adsorption layer thickness. In scenarios where the wall free energy is prominent, the substrate wettability dictates the depletion behavior, resulting in a composition exhibiting exponential decay, aligning well with de Gennes' theory. Conversely, when interfacial tension dominates, the composition at the depletion/adsorption layer adheres to the hyperbolic tangent function, consistent with Cahn's theory. With changes in temperature, both substrate wettability and interfacial tension are modified, thereby manifesting an interplay of influences on the depletion/adsorption behavior.

Furthermore, we have explored the depletion/adsorption behaviors of systems far from equilibrium. Notably, a depletion/adsorption layer, significantly thicker than that observed in equilibrium fluid cases, forms only when the initial composition enters the spinodal region. In such scenarios, the layer thickness is intricately related to both the initial composition and the curvature of the phases. Different curvatures induce the Ostwald-ripening effect, leading to material diffusion and consequential changes in the layer thickness. This indicates that the depletion/adsorption in non-equilibrium fluid systems is governed by both phase separation and the Ostwald-ripening effect which cannot be fully described by de Gennes and Cahn's theories for the equilibrium systems. We anticipate that our study employing phase-field methods contributes to a deeper understanding of the underlying mechanisms governing the depletion/adsorption behavior in multicomponent fluids.

Acknowledgements

H.d.Z. thanks the funding of the research by the Gottfried-Wilhelm Leibniz prize NE 822/31-1 of the German Research Foundation (DFG). H.m.Z. thanks the German Research Foundation (DFG) in the frame of the Research Training Group 2561: Materials Compounds from Composite Materials for Applications in Extreme Conditions for the funding. F.W. is grateful to the VirtMat project P09 "Wetting Phenomena" of the Helmholtz association (MSE program no. 43.31.01). The authors acknowledge support by the state of Baden-Wuerttemberg through bwHPC. Open Access funding enabled and organized by Projekt DEAL.

Conflict of Interests

The authors have no conflicts to disclose.

Data Availability Statement

The data that support the findings of this study are available from the corresponding author upon reasonable request.

Keywords: adsorption · depletion · wetting · phase-field method · phase separation

[1] P.-G. De Gennes, *Rev. Mod. Phys.* **1985**, *57*, 827.
[2] D. Bonn, *Curr. Opin. Colloid Interface Sci.* **2001**, *6*, 22.
[3] D. Quéré, *Annu. Rev. Mater. Res.* **2008**, *38*, 71.
[4] F. Wang, Y. Wu, B. Nestler, *Adv. Mater.* **2023**, *35*, 2210745.
[5] R. A. Jones, L. J. Norton, E. J. Kramer, F. S. Bates, P. Wiltzius, *Phys. Rev. Lett.* **1991**, *66*, 1326.
[6] R. Tuinier, J. Dhont, C. De Kruif, *Langmuir* **2000**, *16*, 1497.
[7] L.-T. Yan, X.-M. Xie, *J. Chem. Phys.* **2007**, *126*, 064908.
[8] H. N. Lekkerkerker, R. Tuinier, H. N. Lekkerkerker, R. Tuinier, *Depletion interaction*, Springer **2011**.
[9] J. J. Michels, *ChemPhysChem* **2011**, *12*, 342.
[10] A. Shafir, D. Andelman, R. R. Netz, *J. Chem. Phys.* **2003**, *119*, 2355.
[11] L.-T. Yan, X.-M. Xie, *Macromolecules* **2006**, *39*, 2388.
[12] J. Freitag, D. W. Bahnemann, *ChemPhysChem* **2015**, *16*, 2670.
[13] P. Zhang, *Macromolecules* **2021**, *54*, 3790.
[14] P. G. De Gennes, *Macromolecules* **1981**, *14*, 1637.
[15] C. Allain, D. Ausserre, F. Rondelez, *Phys. Rev. Lett.* **1982**, *49*, 1694.
[16] D. Ausserre, H. Hervet, F. Rondelez, *Macromolecules* **1986**, *19*, 85.
[17] B. Vincent, *Colloids Surf.* **1990**, *50*, 241.
[18] S. J. Park, A. Shakya, J. T. King, *Proc. Natl. Acad. Sci. USA* **2019**, *116*, 16256.
[19] J. W. Cahn, *J. Chem. Phys.* **1977**, *66*, 3667.
[20] F. Wang, H. Zhang, Y. Wu, B. Nestler, *J. Fluid Mech.* **2023**, *970*, A17.
[21] H. Zhang, Y. Wu, F. Wang, B. Nestler, *J. Chem. Phys.* **2023**, *159*, 164701.
[22] F. Wang, B. Nestler, *J. Chem. Phys.* **2021**, *154*, 094704.
[23] D. Jacqmin, *J. Fluid Mech.* **2000**, *402*, 57.
[24] P. Yue, C. Zhou, J. J. Feng, *J. Fluid Mech.* **2010**, *645*, 279.
[25] N. Bala, M. Pepona, I. Karlin, H. Kusumaatmaja, C. Semprebon, *Phys. Rev. E* **2019**, *100*, 013308.
[26] H. Liang, H. Liu, Z. Chai, B. Shi, *Phys. Rev. E* **2019**, *99*, 063306.
[27] R. Christianto, Y. Rahmawan, C. Semprebon, H. Kusumaatmaja, *Physical Review Fluids* **2022**, *7*, 103606.
[28] H. Zhang, F. Wang, B. Nestler, *Phys. Rev. E* **2023**, *108*, 054121.
[29] F. Wang, O. Tschukin, T. Leisner, H. Zhang, B. Nestler, M. Selzer, G. C. Marques, J. Aghassi- Hagmann, *Acta Mater.* **2020**, *192*, 20.
[30] F. Wang, B. Nestler, *Scr. Mater.* **2016**, *113*, 167.
[31] Y. Wu, F. Wang, S. Zheng, B. Nestler, *Soft Matter* **2024**, *20*, 1523.
[32] F. Wang, B. Nestler, *Phys. Rev. Lett.* **2024**, *132*, 126202.
[33] F. Wang, A. Choudhury, C. Strassacker, B. Nestler, *J. Chem. Phys.* **2012**, *137*, 034702.
[34] H. Zhang, Y. Wu, F. Wang, F. Guo, B. Nestler, *Langmuir* **2021**, *37*, 5275.
[35] H. Zhang, F. Wang, L. Ratke, B. Nestler, *Phys. Rev. E* **2024**, *109*, 024208.
[36] H. Zhang, F. Wang, B. Nestler, *Journal of Computational Physics* **2024**, *505*, 112907.
[37] P. J. Flory, *J. Chem. Phys.* **1942**, *10*, 51.
[38] H. Zhang, F. Wang, B. Nestler, *Langmuir* **2022**, *38*, 6882.
[39] G. Whyman, E. Bormashenko, T. Stein, *Chem. Phys. Lett.* **2008**, *450*, 355.

Manuscript received: January 29, 2024
Revised manuscript received: April 22, 2024
Accepted manuscript online: April 25, 2024
Version of record online: ■■, ■■

RESEARCH ARTICLE

When an equilibrium binary fluid contacts a rigid solid substrate, microscopic depletion/adsorption layers are formed; the thickness of the layers is decided by the substrate wettability, fluid-fluid interfacial tension, and temperature. For the non-equilibrium system, a thicker macroscopic depletion/adsorption layer is induced by the wetting effect, attributing to the associated phase separation.

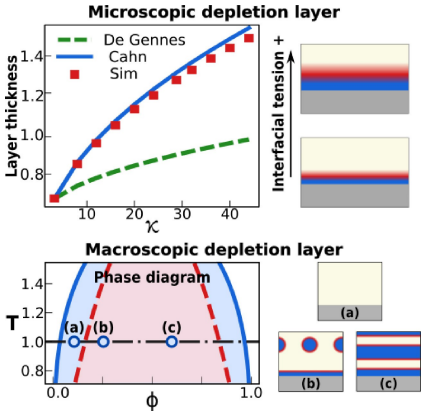

H. Zhang, H. Zhang, F. Wang, B. Nestler*

1 – 12

Wetting Effect Induced Depletion and Adsorption Layers: Diffuse Interface Perspective